JOM, Vol. 75, No. 4, 2023
https://doi.org/10.1007/s11837-022-05632-2




# Effect of $Al_2O_3$ on Viscosity and Structure of $SiO_2$-FeO-$Al_2O_3$-$Fe_2O_3$-CaO-MgO Slag System

BAOREN WANG,[1,2] HONGYING YANG,[1,2] ZHENAN JIN,[1,2,4] TIANHAO ZHENG,[1,2] GUOBAO CHEN,[1,2] and ZHUNQIN DONG[3]

1.—Key Laboratory for Ecological Metallurgy of Multi-metallic Mineral of Education Ministry, Northeastern University, Shenyang 110819, China. 2.—School of Metallurgy, Northeastern University, Shenyang 110819, China. 3.—Shandong Humon Smelting Co. Ltd., Yantai 264109, China. 4.—e-mail: jinzn@smm.neu.edu.cn

In this study, the effect of $Al_2O_3$ content on viscous behaviors of the secondary copper smelting slags was investigated in depth. It was determined that in the slag system of $SiO_2$-FeO-$Al_2O_3$-12 wt.%$Fe_2O_3$-8 wt.%CaO-3 wt.%MgO, the addition of $Al_2O_3$ (0–12 wt.%) increased the slag viscosity and activation energy for viscous flow ($E_\eta$). The breaking temperature of the slag ($T_{Br}$) exhibited a minimum value at the $Al_2O_3$ addition of 6 wt.%. X-ray diffraction (XRD) tests and thermodynamic calculations indicated the increase of $Al_2O_3$ content can promote the precipitation of fayalite and anorthite phases and simultaneously suppress the precipitation of clinopyroxene phase. Moreover, Fourier transform infrared (FTIR) and Raman spectroscopy suggested that $Al_2O_3$ presented acidic oxide properties and acted as a network former to increase the polymerization of the melt. As the $Al_2O_3$ increased, the aluminium–oxygen tetrahedra copolymerized with silicon–oxygen tetrahedra, forming a more complex aluminosilicate composite network structure.

## INTRODUCTION

At present, among the mainstream copper production technologies in the world, the oxygen-enriched bottom-blow melting process is widely used because of its unparalleled advantage in the comprehensive recovery of valuable metals. As copper matte is a good melting agent for precious metals, most of the precious metals are enriched into the copper matte under the vigorous stirring of oxygen, thus realizing the recovery of gold and silver. In China, most heavy non-ferrous smelting enterprises, such as Shandong Humon Smelting Co., Ltd., Henan Zhongyuan Gold Smelter, are using this technology to produce gold and silver as by-products. However, in recent years, secondary resources containing higher grade Au and Ag have become an important source of ingredients for the copper industry due to the decrease in the quantity of high-quality gold concentrates. Based on the adaptability of the oxygen-enriched bottom-blow smelting to raw materials, secondary resources can be directly dispensed into the copper smelting furnaces for collaborative smelting, which can not only recover the gold and silver but also realize the resourcefulness and harmlessness of the secondary resources. However, the addition of secondary resources inevitably introduces a large amount of gangue such as $Al_2O_3$ and $SiO_2$, which increases the slag volume and deteriorates the working condition of the copper smelting furnace. As an important indicator of the smooth smelting process, viscosity not only affects the rate of mass and heat transfer but also relates to whether the metal or matte can be adequately separated by the slag layer settlement.[1–4] The allotment of secondary resources can make $Al_2O_3$ content in the slag reach high levels, which in turn affects the slag viscosity. Therefore, it is necessary to study the effect of $Al_2O_3$ on viscous behaviors of the secondary copper smelting slags, which is meaningful for reducing the copper content in slag and improving the operational stability and production efficiency.

(Received September 12, 2022; accepted November 27, 2022; published online December 22, 2022)

So far, a tremendous amount of work has been done by scholars to investigate the effect of $Al_2O_3$ on slag viscosity.[5–17] In the ternary $Na_2O$-$Al_2O_3$-$SiO_2$ system, Mohri et al.[5] concluded that $Al^{3+}$ increases the melt viscosity by binding $[SiO_4]^{4-}$ monomers and randomly building three-dimensional network structures. Kim et al.[6] investigated the action of $Al_2O_3$ on the viscosity of a quaternary slag system (CaO-$SiO_2$-MgO-$Al_2O_3$) and found that at different alkalinity ($CaO/SiO_2$), increasing $Al_2O_3$ led to a gradual polymerization of the aluminate structure in the slag, which increased the slag viscosity. In the same system, Talapaneni et al.[7] suggested that the addition of $Al_2O_3$ copolymerized the silicate network structure with the aluminate network structure to form a highly polymerized composite aluminosilicate, leading to higher viscosity. In addition, in the CaO-$SiO_2$-FeO-$CaF_2$ system,[8] CaO-$SiO_2$-8 wt.%MgO-$Al_2O_3$-5 wt.%$TiO_2$ system,[9] CaO-$SiO_2$-$Al_2O_3$-MgO-$Fe_tO$ system[10–12] and CaO-$SiO_2$-$Al_2O_3$-11.30 wt.%MgO-6.93 wt.%$TiO_2$-0.11 wt.%$V_2O_5$ system,[13] $Al_2O_3$ acts as an acidic oxide and the melt viscosity increases with its content. However, Park et al.[14] found that $Al_2O_3$ exhibited amphoteric oxide properties in both the ternary and quaternary systems by determining the viscosity of CaO-$SiO_2$-(MgO)-$Al_2O_3$ melt. Prior to the addition of 10 wt.% $Al_2O_3$, it was present as a network former, while at levels > 10 wt.% it acted as a network modifier and depolymerized the silicate structure. Furthermore, Park et al. also thermodynamically verified the amphoteric behavior of $Al_2O_3$ by considering the activity coefficient of $Al_2O_3$ in the melt.[15] Similarly, the amphoteric behavior of $Al_2O_3$ was found in the CaO-$SiO_2$-$Al_2O_3$-8 wt.%MgO-5 wt.%FeO-10 wt.%$TiO_2$ system by Li et al.[16] The slag viscosity reached a maximum at the addition of 15 wt.% $Al_2O_3$ and then decreased. The researchers proposed that the amphoteric behavior of $Al_2O_3$ mainly depended on the composition of slag. When the molar ratio of $Al_2O_3$ to the sum of all other basic oxides in the slag was < 1, $Al_2O_3$ was a network former, and vice versa as a network-modified body.[17] However, in the investigation of slag viscosity, a great deal of exploration and generally recognized conclusions have focused on calcium silicate-based slags, while little research has been done on iron silicate-based slags, especially those with high FeO and $Fe_2O_3$ content. As we know, copper smelting slag belongs to iron-silicate based slag, so it is instructive to clarify the role of $Al_2O_3$ in iron-silicate based slag for co-smelting.

In this study, the slag viscosity of the $SiO_2$-FeO-$Al_2O_3$-12 wt.%$Fe_2O_3$-8 wt.%CaO-3 wt.%MgO system was determined via the rotating cylinder method. Furthermore, the effects of $Al_2O_3$ content on slag viscosity, slag phase relationship, breaking temperature of the slag ($T_{Br}$) and activation energy for viscous flow ($E_\eta$) were investigated in depth. On this basis, Fourier transform infrared (FTIR) (VERTEX70, Bruker, Germany) and Raman (HR800, Jobin Yvon, France) spectroscopies were applied to characterize the slag structure. This article will provide valuable suggestions and guidance for the synergetic treatment of secondary resources in copper industrial processes.

## EXPERIMENTAL

### Sample Preparation

The chemical reagents $Fe_2O_3$, $SiO_2$, CaO, $Al_2O_3$, MgO and Fe powder were all analytical purity. The reagents were accurately weighted and uniformly mixed according to the compositions set in Table I. FeO was obtained on site by mixing Fe and $Fe_2O_3$ powders in a 1:1 molar ratio. The ratio of $Fe/SiO_2$ was fixed at 1.0, which represented the mass ratio of total Fe to $SiO_2$ in the sample. Under the protection of argon atmosphere, the samples in the molybdenum crucible were pre-melted at 1773 K for about 2 h to obtain a water-quenched slag. For the determination of total and divalent iron, the traditional potassium dichromate titration method was used for the analysis. The content of trivalent iron was obtained by subtracting the divalent iron from total iron. According to the results in Table I, there are no significant changes in the chemical composition of the samples before and after pre-melting obtained by x-ray fluorescence spectroscopy (XRF, ZSX PrimusII, Rigaku Corp., Japan). The $Fe_2O_3$ content of the samples increased slightly after pre-melting, which may be due to the oxidation of FeO.

### Experimental Apparatus and Procedure

In the present study, the rotating cylinder method was used to determine the viscosity. The equipment used in the experiments has been described in detail in our previous work.[18,19] To prevent contamination of the slag, the crucibles and spindles used were made of molybdenum. The viscometer (DV2TRV, Brookfield Engineering Labs., Inc, Middleborough, MA, USA) was calibrated with different values of reference castor oil prior to the measurements.

Approximately 180 g of quenched slag obtained by pre-melting was put into a molybdenum crucible for viscosity testing. The crucible was placed in the constant temperature zone of the tube furnace. Subsequently, 0.4 L/min of Ar gas was introduced into the furnace chamber. The furnace was then heated up to 1773 K according to the set program and kept for 1 h. The depth of melt pool was around 40 mm. During the heat preservation period, the slag was homogenized at regular intervals by stirring with a fine molybdenum wire deep into the melt pool. At the end of the holding time, the rotating spindle was dipped into the melt with the probe 10 mm from the bottom of the melt pool.

The viscosity test was performed by continuous cooling from 1773 K at a rate of 3 K/min. The spindle speed was fixed at 12 r/min. The viscosity test was stopped when the tested viscosity value

**Table I. Experimental compositions of the synthesized slags in the current study**

| | Designed composition (wt.%) | | | | | | | Analyzed composition (wt.%) | | | | | | |
|---|---|---|---|---|---|---|---|---|---|---|---|---|---|---|
| No. | $Fe/SiO_2$ | $SiO_2$ | FeO | $Fe_2O_3$ | MgO | $Al_2O_3$ | CaO | $Fe/SiO_2$ | $SiO_2$ | FeO | $Fe_2O_3$ | MgO | $Al_2O_3$ | CaO |
| 1 | 1.0 | 38.40 | 38.60 | 12 | 3 | 0 | 8 | 1.03 | 37.48 | 38.16 | 12.81 | 2.93 | 0 | 7.88 |
| 2 | 1.0 | 37.09 | 36.91 | 12 | 3 | 3 | 8 | 1.03 | 36.06 | 36.23 | 12.73 | 2.96 | 3.08 | 8.04 |
| 3 | 1.0 | 35.77 | 35.23 | 12 | 3 | 6 | 8 | 1.02 | 35.14 | 34.91 | 12.39 | 2.90 | 6.21 | 7.79 |
| 4 | 1.0 | 34.46 | 33.54 | 12 | 3 | 9 | 8 | 1.03 | 33.52 | 33.12 | 12.66 | 3.01 | 8.96 | 7.86 |
| 5 | 1.0 | 33.15 | 31.85 | 12 | 3 | 12 | 8 | 1.01 | 32.80 | 31.04 | 12.92 | 2.84 | 11.83 | 7.91 |

**Table II. The chemical compositions of slags after viscosity experiments (wt.%)**

| No | $Fe/SiO_2$ | $SiO_2$ | FeO | $Fe_2O_3$ | MgO | $Al_2O_3$ | CaO |
|---|---|---|---|---|---|---|---|
| 1 | 1.03 | 37.21 | 37.34 | 13.35 | 2.95 | 0 | 7.67 |
| 2 | 1.03 | 35.88 | 35.72 | 12.98 | 2.92 | 3.11 | 7.88 |
| 3 | 1.02 | 34.86 | 34.13 | 13.06 | 2.84 | 5.87 | 7.82 |
| 4 | 1.04 | 33.35 | 32.49 | 13.42 | 2.87 | 8.65 | 7.69 |
| 5 | 1.02 | 32.54 | 30.34 | 13.53 | 2.78 | 12.06 | 7.74 |

reached the limit of the instrument. At this time, the furnace was reheated to 1773 K, and then the spindle was lifted out of the melt pool. Maintaining for 30 min, a thin molybdenum rod was immersed in the melt pool and then quickly removed for quenching. This process was repeated several times to accumulate samples for subsequent structural characterization. After quenching, the remaining slag was cooled with the furnace under Ar gas.

Table II lists the experimental components of slag after viscosity measurement. It can be seen that except for the relative changes of FeO and $Fe_2O_3$, the chemical compositions of the other components in the slag are not much different from those of the pre-melted slag. During viscosity measurement, although 0.4 L/min argon gas was introduced, the system could not be completely sealed because of the stirring of molybdenum spindle. FeO is further oxidized to a portion of $Fe_2O_3$. Notably, molybdenum crucible and spindle are used in the experiments, and molybdenum inevitably enters the slag, accounting for about 1–1.5 wt.% ($MoO_3$). Since the percentage of molybdenum is very small, it is negligible in the viscosity experiments.

## RESULTS AND DISCUSSION

### Effect of $Al_2O_3$ on Breaking Temperature and Slag Viscosity

The viscosity dependence of $SiO_2$-FeO-$Al_2O_3$-12 wt.%$Fe_2O_3$-8 wt.%CaO-3 wt.%MgO slag system with temperature at different $Al_2O_3$ contents is illustrated in Fig. 1. As expected, for all slag samples, the viscosity increases smoothly at high temperatures as the temperature decreases. The

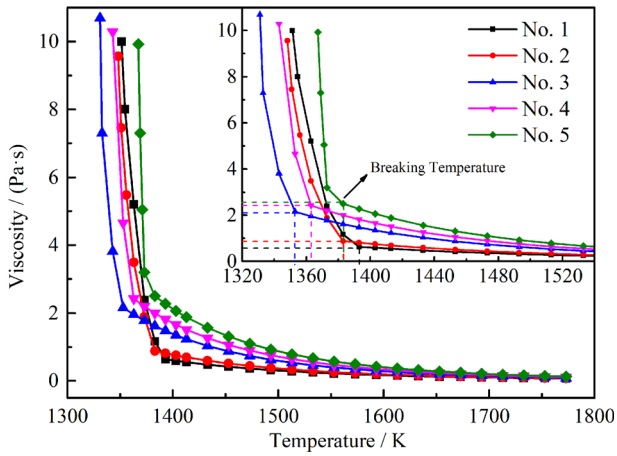


Fig. 1. Viscosity of the $SiO_2$-FeO-$Al_2O_3$-12 wt.%$Fe_2O_3$-8 wt.%CaO-3 wt.%MgO system as a function of temperature.

increase in viscosity becomes sharply larger below a specific temperature. This abrupt change point, commonly referred to the breaking temperature ($T_{Br}$), has been marked in Fig. 1. It is observed that with the increase of $Al_2O_3$ content, the $T_{Br}$ of slag shows a trend of first decreasing and then increasing. With the initial increase of $Al_2O_3$ content to 3 wt.%, $T_{Br}$ has a slight downward trend. The subsequent addition of $Al_2O_3$ causes a significant decrease in the $T_{Br}$ of slag. However, when the $Al_2O_3$ content further increases to 9 wt.%, the $T_{Br}$ of slag exhibits the opposite trend. This nonlinear variation is consistent with the work reported by Wang et al.[11] and Zhao et al.,[20] which is attributed to the difference in the crystallization behavior of slags with different compositions.

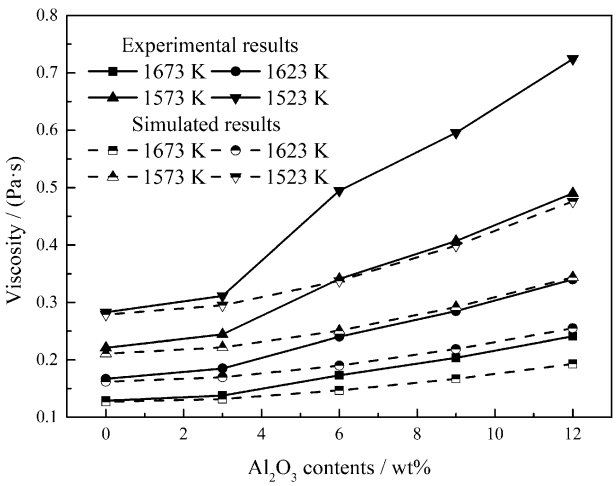


Fig. 2. Dependence of slag viscosity on $Al_2O_3$ content at different temperatures.

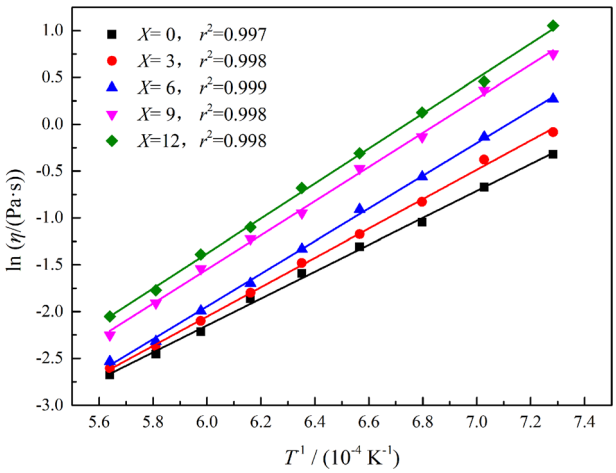


Fig. 3. The ln$\eta$ and 1/$T$ fitting results of the $SiO_2$-FeO-$X$ wt.%$Al_2O_3$-12 wt.%$Fe_2O_3$-8 wt.%CaO-3 wt.%MgO slags.

Figure 2 shows the dependence of slag viscosity on $Al_2O_3$ content at different temperatures. It can be noted that the slag viscosity gradually increases with the addition of $Al_2O_3$. This indicates that $Al_2O_3$ exhibits acidic oxide properties in this slag system, namely as a network-forming body that absorbs free oxygen anions ($O^{2-}$) and forms complexed anions. It is worth pointing out that the effect of $Al_2O_3$ on increasing slag viscosity is more remarkable in the low temperature range and at high $Al_2O_3$ content, while it becomes weaker at high temperatures and low $Al_2O_3$ content. For example, at a lower temperature of 1523 K, the viscosity of the slag increases significantly by 0.44 Pa s as the $Al_2O_3$ content increases from 0 wt.% to 12 wt.%, while at 1673 K, the same situation increases by only 0.11 Pa s. This trend can be clearly seen from the slope in Fig. 2. On the other hand, the slag viscosity increased by 0.03 Pa s at 1523 K as the $Al_2O_3$ content varied in the lower range (0–3 wt.%) and by 0.18 Pa s when its content continued to increase to higher levels (3–6 wt.%). The increase was about 6.0 times greater than the former.

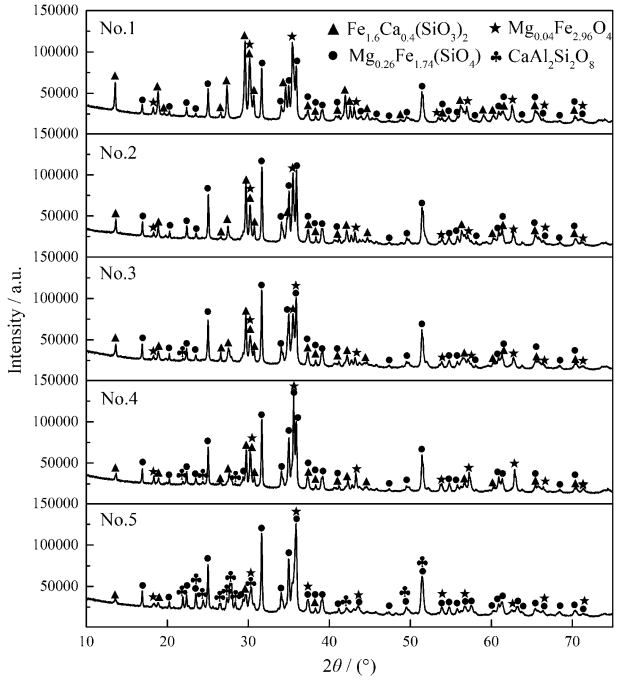


Fig. 4. XRD patterns of slow cooling slag with different $Al_2O_3$ contents.

In the iron-silicate slag system, there are many complex silica–oxygen anion groups. At the same time, $Al_2O_3$ absorbs $O^{2-}$ in the melt to form corresponding complex anions, such as $[AlO_2]^-$ and $[AlO_3]^{2-}$, which are embedded in the silicate network structure to form more polymeric complex anion groups. With the increasing $Al_2O_3$ content, there are more and more complex anion clusters, which makes the network structure of the melt more complex, and thus the viscosity changes significantly at high $Al_2O_3$ content. Additionally, the network structure of the melt is capable of being destroyed by the thermal energy that high temperatures have.[6,21] Therefore, the effect of increasing $Al_2O_3$ on the melt polymerization is not significant at higher temperatures. Also, Fig. 2 illustrates the effect of $Al_2O_3$ on the melt viscosity calculated by thermodynamic package Factsage 8.1.[22] The results of the software simulation show the same direction of change as the actual measurement. With the increase of $Al_2O_3$ content, the viscosity increases, but the calculated values are relatively lower than the measured values. This can be attributed to the partial oxidation of FeO to $Fe_2O_3$ during the high temperature measurements.[23–25]

Using the Arrhenius formula,[26] the dependence of melt viscosity on temperature can be obtained as shown in Eq. 1:

$$\eta = A \exp(E_\eta / RT) \quad (1)$$

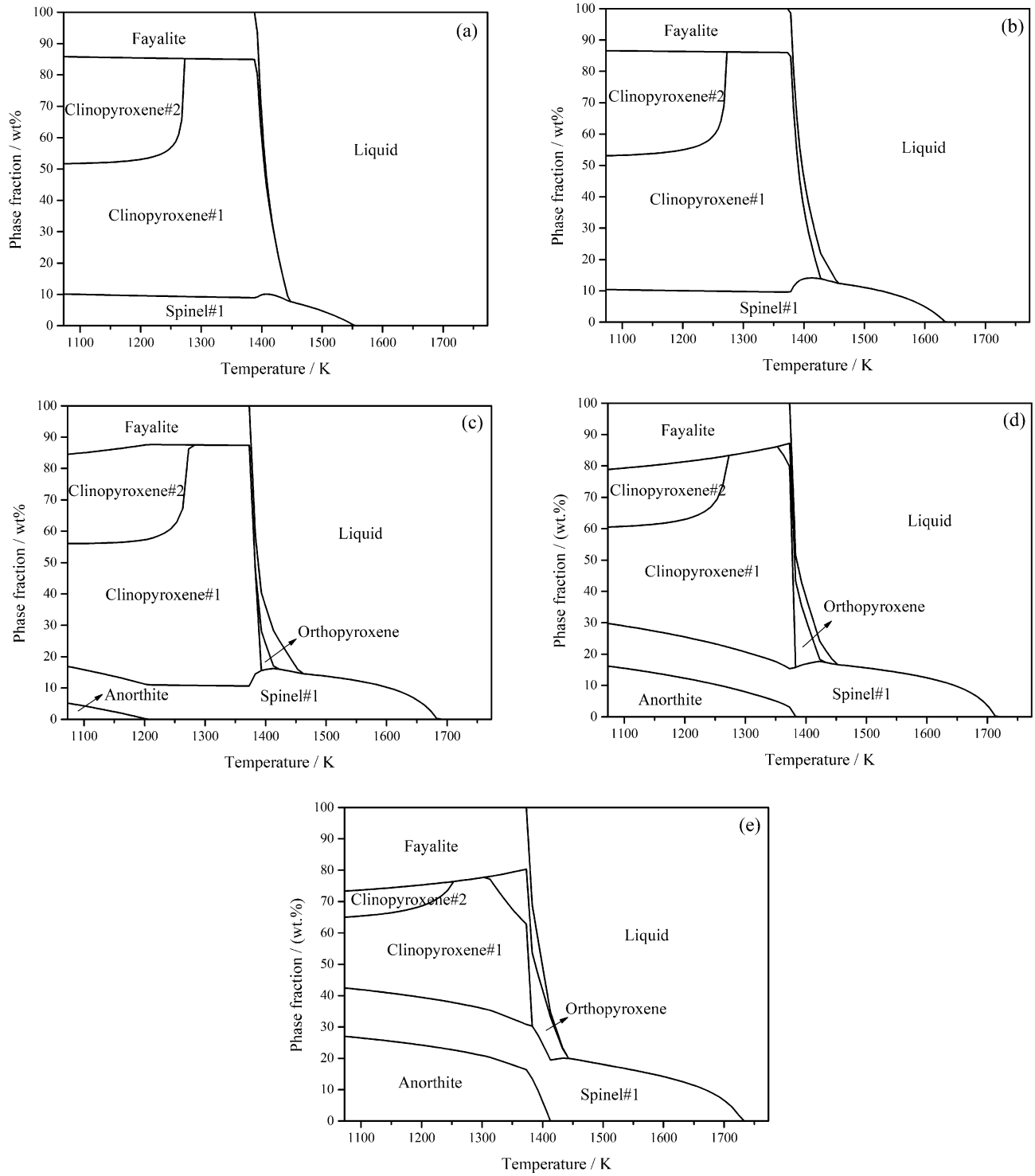


Fig. 5. Calculated phase equilibrium of slag system by Factsage 8.1 at 1073–1773 K, with various $Al_2O_3$ contents of (a) 0 wt.%, (b) 3 wt.%, (c) 6 wt.%, (d) 9 wt.% and (e) 12 wt.%.

where $\eta$ is the viscosity, Pa s; $A$ is the pre-exponential constant; $E_\eta$ is the activation energy for viscous flow, J $mol^{-1}$.

The variations in the natural logarithm of the viscosity ($\ln\eta$) versus the reciprocal of temperature ($1/T$) for varying $Al_2O_3$ contents are given in Fig. 3. It can be clearly seen that for all slag compositions, $\ln\eta$ is highly linearly correlated with $1/T$, indicating the melt at high temperatures follows Arrhenius behavior. The $E_\eta$ values can be easily obtained from the slope of the straight line in Fig. 3. The

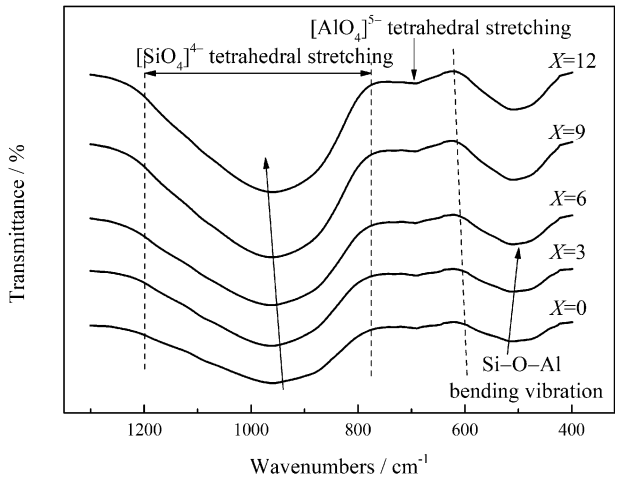


Fig. 6. FTIR plots of quenched slags of $SiO_2$-FeO-*X* wt.%$Al_2O_3$-12 wt.%$Fe_2O_3$-8 wt.%CaO-3 wt.%MgO system at different $Al_2O_3$ contents.

calculated $E_\eta$ values were 119.45 kJ mol$^{-1}$ (0 wt.%), 130.32 kJ mol$^{-1}$ (3 wt.%), 145.11 kJ mol$^{-1}$ (6 wt.%), 151.53 kJ mol$^{-1}$ (9 wt.%) and 155.30 kJ mol$^{-1}$ (12 wt.%), respectively. As expected, the $E_\eta$ increases with increasing $Al_2O_3$ content, causing the viscosity to be more sensitive to temperature fluctuations and the thermal stability of the slag system less stable. This is mainly because the increase in $Al_2O_3$ leads to increasingly complex ($Si[Al]_xO_y^{n-}$) viscous units in the melt. As a result, the energy barrier required to move the mass in the slag from one equilibrium position to another equilibrium position is larger, i.e., the activation energy increases and the thermal stability of the slag system becomes worse. The results of the variations in $E_\eta$ values are consistent with the changes of slag viscosity.

## Effect of $Al_2O_3$ on Phase Relations

Figure 4 shows the x-ray diffraction (XRD) patterns of slow-cooled slag at varying $Al_2O_3$ contents. It is obvious that the slag possesses better crystalline properties under the conditions of cooling with the furnace. In the absence of $Al_2O_3$, the solid phases precipitated from the slag are clinopyroxene ($Fe_{1.6}Ca_{0.4}(SiO_3)_2$), spinel ($Mg_{0.04}Fe_{2.96}O_4$) and fayalite ($Mg_{0.26}Fe_{1.74}(SiO_4)$). With the increase in $Al_2O_3$ content, the intensity of diffraction peaks of clinopyroxene phase decreases significantly, while that of fayalite phase increases remarkably. For the spinel phase, there is also an increase in the intensity of the diffraction peaks. Additionally, the diffraction peak of anorthite ($CaAl_2Si_2O_8$) appears in the XRD pattern when the $Al_2O_3$ content is increased to 6 wt.%. As the $Al_2O_3$ content continues to increase to 12 wt.%, the diffraction peak of clinopyroxene phase almost disappears, and yet the intensity of the anorthite phase further increases. The above results suggest that increasing $Al_2O_3$ content can promote the precipitation of fayalite phase and snorthite phase and suppress the precipitation of clinopyroxene phase.

To further understand the correlation between the slag phases and $Al_2O_3$ content, the phase equilibrium calculations of the system in the temperature range of 1073–1773 K were carried out using Factsage software (Equilib module, Fact PS and FT Oxid databases), and the results are shown in Fig. 5a–e. Three thermodynamic main phases, fayalite, clinopyroxene and spinel, are present in the slag without the addition of $Al_2O_3$. As the $Al_2O_3$ content increases from 0 wt.% to 12 wt.%, the phase equilibrium fraction of fayalite keeps increasing and the phase fraction of clinopyroxene gradually decreases, consistent with the XRD results. At the $Al_2O_3$ addition of 6 wt.%, orthopyroxene and anorthite phases started to precipitate in the slag and their phase fractions increase further with the increase of $Al_2O_3$ content. However, no diffraction peaks of the orthopyroxene phase are observed in the XRD results. This may be due to the low relative content of the orthopyroxene phase, which fails to reach the detection limit of the instrument. It should be noted that the calculated results are only ideal values to verify the XRD results, and the actual process of precipitation may also be related to the cooling conditions as well as the alkalinity of the system.

## FTIR and Raman Spectroscopy Analysis

Figure 6 shows the infrared spectra of quenched samples with different $Al_2O_3$ contents. It is obvious that the vibration intensity of the $[SiO_4]^{4-}$ band (1200–750 cm$^{-1}$)[27] gradually increases with increasing $Al_2O_3$ content, which is reflected by the deepening of the groove depth. This is due to the incorporation of a large amount of $[AlO_4]^{5-}$ tetrahedra (750–590 cm$^{-1}$)[16,28] into the $[SiO_4]^{4-}$ tetrahedra, forming a more complex aluminosilicate composite structure. This can also be verified by the gradual deepening of the vibration depth in the Si-O-Al band at 500 cm$^{-1}$,[29] indicating a gradual increase in the bond between the $[SiO_4]^{4-}$ tetrahedra and $[AlO_4]^{5-}$ tetrahedra. In general, when $Al_2O_3$ behaves as a network former, the width of the $[SiO_4]^{4-}$ vibration band should become narrower as its content increases steadily. However, there was no significant change in the present study. This may be due to the fact that the addition of $Al_2O_3$ reduces the absolute amount of $SiO_2$ in the slag, thus decreasing the relative amount of $[SiO_4]^{4-}$ in the melt. In addition, the vibrational intensity of $[AlO_4]^{5-}$ located in the range of 750–590 cm$^{-1}$ also gradually increases, which further indicates that $Al_2O_3$ presents as a network former and increases the polymerization of the melt. Moreover, the center of gravity of the vibration band of the silica–oxygen tetrahedron tends to become larger. This suggests that with the addition of $Al_2O_3$, the structure of the silicate complex anion becomes more complex with

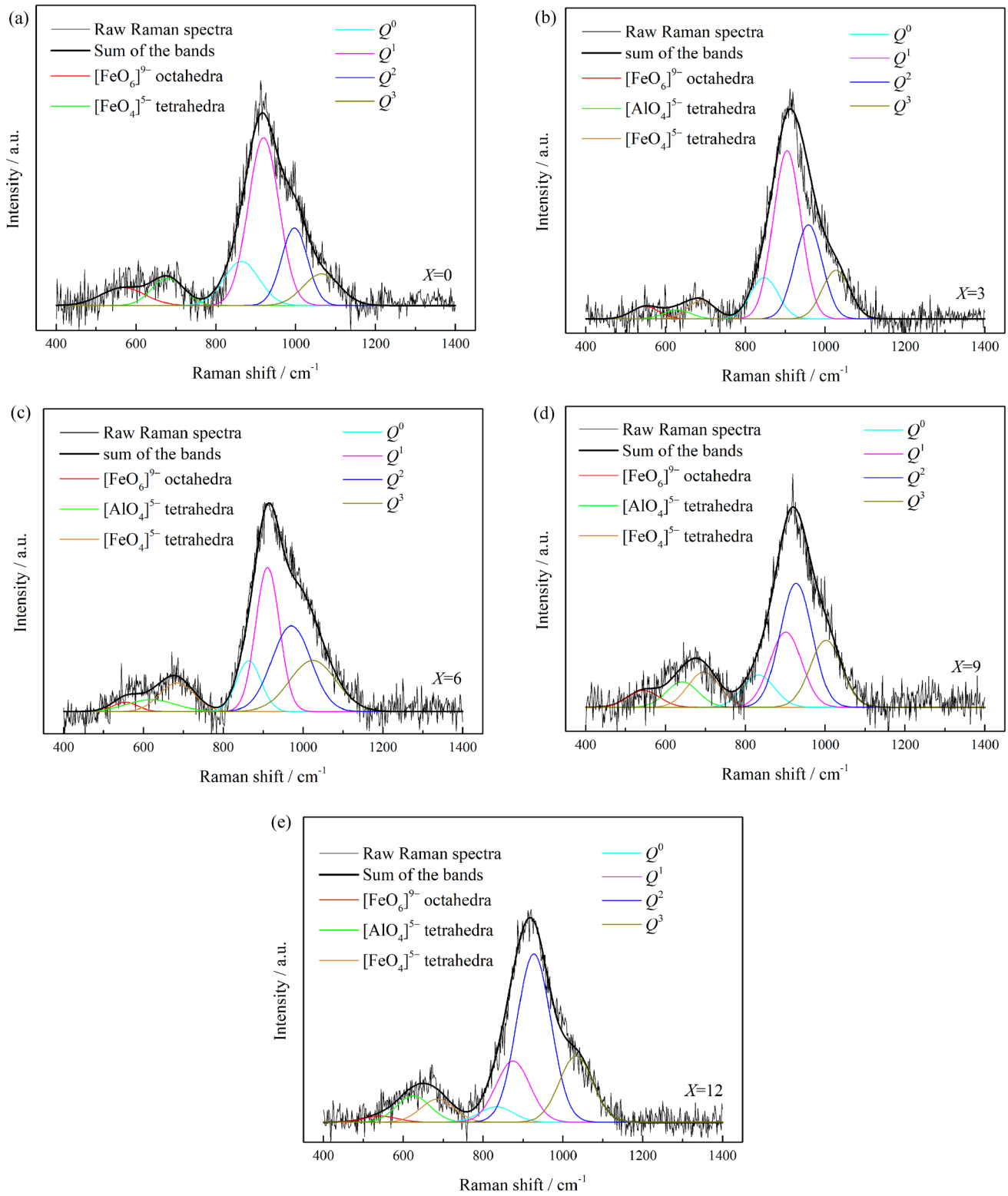


Fig. 7. Deconvoluted Raman spectrum of $SiO_2$-FeO-*X* wt.%$Al_2O_3$-12 wt.%$Fe_2O_3$-8 wt.%CaO-3 wt.%MgO system at different $Al_2O_3$ contents.

more structural units in the form of chains and sheets, while the relative proportion of structural units in monomers and dimers decreases. Therefore, the experimentally measured viscosity strongly depends on the structural role of $Al_2O_3$ in the melt. In the present study, no vibrational peaks of $[AlO_6]^{9-}$ octahedra were observed. In such a slag system with many basic oxides, there are enough cations for charge compensation, which favors the presence of $[AlO_4]^{5-}$ tetrahedra.

As an effective means of characterizing the microstructure of quenched slag, Raman spectra of the samples are given in Fig. 7 and deconvoluted by applying the method of Mysen et al.[30,31] Raman curves have distinct vibrational bands in both low and high wavelengths, corresponding to $[FeO_6]^{9-}$ octahedral vibration band (550 $cm^{-1}$),[32] $[AlO_4]^{5-}$ tetrahedral vibration band (630 $cm^{-1}$), $[FeO_4]^{5-}$ tetrahedral vibration band (690 $cm^{-1}$)[12,33] and $[SiO_4]^{4-}$ tetrahedral vibration band (800–1200 $cm^{-1}$), respectively. With the addition of $Al_2O_3$, the vibrational peak of $[AlO_4]^{5-}$ tetrahedron appears and its integral area increases with the increase of $Al_2O_3$. Referring to our and other scholars' previous research,[18,34,35] the amount of non-bridging oxygen (NBO/Si) in the melt is used to determine the polymerization degree of the melt, and then the viscosity of the melt is evaluated. NBO/Si can be determined by multiplying the mole fraction of structural units ($Q^n$) of different types of silicon–oxygen tetrahedrons in the melt by their corresponding non-bridged oxygen number ($n$), as shown in Eqs. 2 and 3:

$$X_{Q^i} = A_{Q^i} \Big/ \sum_{i=0}^{3} A_{Q^i} \tag{2}$$

$$\mathrm{NBO/Si} = 4X_{Q^0} + 3X_{Q^1} + 2X_{Q^2} + X_{Q^3} \tag{3}$$

where $X_{Q^i}$ is the molar fraction of $Q^i$; $A_{Q^i}$ is the Raman band area of $Q^i$ ($i$ = 0–3).

By deconvoluting the Raman spectrum, the semi-quantitative values of the molar fraction of structural units in the melt can be obtained. The variations in their values with $Al_2O_3$ content are presented in Fig. 8. With the increase of $Al_2O_3$, the molar fraction of $Q^0$ and $Q^1$ in the silicate melt decreases, while that of $Q^2$ and $Q^3$ increases. In particular, the changes of $Q^1$ and $Q^2$ are obvious, indicating that the changes of the polymerization degree of the silicate network are mainly controlled by the depolymerization of the chain-like units. As expected, the molar fraction of $[AlO_4]^{5-}$ structural units gradually increases with the addition of $Al_2O_3$, suggesting that $Al_2O_3$ existed in the iron-silicate melt as a network-former, increasing the degree of polymerization of the melt. The variation in the Raman spectrum of the quenched slag is consistent with the changes in the FTIR spectrum and viscosity of the slag.

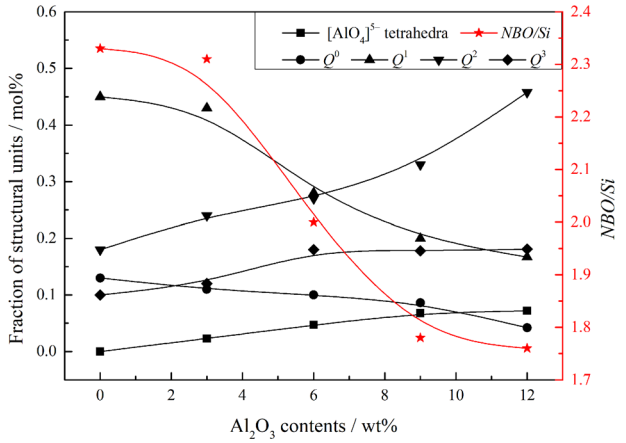


Fig. 8. Variations in molar fraction of various structural units in Raman spectra with $Al_2O_3$ content.

## CONCLUSION

(1) The viscosity and the activation energy for viscous flow of the co-smelting slag both increased with the addition of $Al_2O_3$ (0–12 wt.%). The initial increase of $Al_2O_3$ (0–6 wt.%) decreased the $T_{Br}$ of the slag, and yet continued increases (6–12 wt.%) led to the opposite trend.

(2) The increase of $Al_2O_3$ content promoted the precipitation of fayalite and anorthite phases as well as inhibited the precipitation of clinopyroxene phase, which can be confirmed by XRD and Factsage software.

(3) $Al_2O_3$ presented acidic oxide properties and acted as a network former to increase the polymerization of the melt. Forming a more complex aluminosilicate composite structure was correlated with an increase in $Al_2O_3$ content.

## ACKNOWLEDGEMENTS

The authors are grateful for the financial supports from the National Key R&D Program of China (2018YFC1902004, 2018YFC1902002).

## CONFLICT OF INTEREST

The authors declare that they have no conflict of interest.

## REFERENCES

1. A. Shankar, M. Gornerup, A.K. Lahiri, and S. Seetharaman, *Metall. Mater. Trans. B* 38, 911 (2007).
2. J.H. Park, *Metall. Mater. Trans. B* 44, 938 (2013).
3. M. Chen, S. Raghunath, and B. Zhao, *Metall. Mater. Trans. B* 46, 577 (2015).
4. A. Kondratiev, E. Jak, and P.C. Hayes, *JOM* 54, 41 (2002).
5. M. Mohri, Y. Sasaki, and K. Ishii, *ISIJ Int.* 41, 410 (2001).
6. H. Kim, H. Matsuura, F. Tsukihashi, W. Wang, D.J. Min, and I. Sohn, *Metall. Mater. Trans. B* 44, 5 (2013).

7. T. Talapaneni, N. Yedla, S. Pal, and S. Sarkar, *Metall. Mater. Trans. B* 48, 1450 (2017).
8. F. Shahbazian, D. Sichen, and S. Seetharaman, *ISIJ Int.* 42, 155 (2002).
9. Z. Yan, X. Lv, J. Zhang, Y. Qin, and C. Bai, *Can. Metall. Q.* 55, 186 (2016).
10. J.R. Kim, Y.S. Lee, D.J. Min, S.M. Jung, and S.H. Yi, *ISIJ Int.* 44, 1291 (2004).
11. Z. Wang, Y. Sun, S. Sridhar, M. Zhang, M. Guo, and Z. Zhang, *Metall. Mater. Trans. B* 46, 537 (2015).
12. Z. Wang, Y. Sun, S. Sridhar, M. Zhang, M. Guo, and Z. Zhang, S. *Metall. Mater. Trans. B* 46, 2246 (2015).
13. C. Feng, M. Chu, J. Tang, Y. Tang, and Z. Liu, *Steel Res. Int.* 87, 1274 (2016).
14. J.H. Park, D.J. Min, and H.S. Song, *Metall. Mater. Trans. B* 35, 269 (2004).
15. J.H. Park, H. Kim, and D.J. Min, *Metall. Mater. Trans. B* 39, 150 (2008).
16. T. Li, C. Sun, S. Song, and Q. Wang, *Metals* 9, 743 (2019).
17. I. Sohn and D.J. Min, *Steel Res. Int.* 83, 611 (2012).
18. B. Wang, H. Yang, Z. Jin, Z. Liu, and M. Zou, *Metals* 12, 24 (2022).
19. J. Lü, Z. Jin, H. Yang, L. Tong, G. Chen, and F. Xiao, *Int. J. Miner. Metall. Mater.* 24, 756 (2017).
20. B. Zhao, E. Jak, and P.C. Hayes, *Metall. Mater. Trans. B* 30, 597 (1999).
21. Y. Gao, S. Wang, C. Hong, X. Ma, and F. Yang, *Int. J. Miner. Metall. Mater.* 21, 353 (2014).
22. C.W. Bale, E. Bélisle, P. Chartrand, S.A. Decterov, G. Eriksson, A.E. Gheribi, K. Hack, I.H. Jung, Y.B. Kang, J. Melançon, A.D. Pelton, S. Petersen, C. Robelin, J. Sangster, P. Spencer, and M. Van Ende, *Calphad: Comput. Coupling Phase Diagr. Thermochem.* 55, 1 (2016).
23. D.B. Dingwell and D. Virgo, *Geochim. et Cosmochim. Acta.* 51, 195 (1987).
24. N. Saito, N. Hori, K. Nakashima, and K. Mori, *Metall. Mater. Trans. B* 34, 509 (2003).
25. J.P. Yu, L.J. Wang, Y.X. Wang, Y.Q. Liu, and G.Z. Zhou, *J. Iron Steel Res.* 26, 1 (2014).
26. Z. Jin, J. Lv, and H. Yang, *Russ. J. Non-Ferr. Met.* 61, 153 (2020).
27. H. Park, J. Park, G.H. Kim, and I. Sohn, *Steel Res. Int.* 83, 150 (2012).
28. W.H. Kim, I. Sohn, and D.J. Min, *Steel Res. Int.* 81, 735 (2010).
29. Y.S. Lee, D.J. Min, S.M. Jung, and S.H. Yi, *ISIJ Int.* 44, 1283 (2004).
30. B.O. Mysen, L.W. Finger, D. Virgo, and F.A. Seifert, *Am. Miner.* 67, 686 (1982).
31. B.O. Mysen, D. Virgo, and C.M. Scanrn, *Am. Miner.* 65, 690 (1980).
32. Z. Jin, H. Yang, J. Lv, L. Tong, G. Chen, and Q. Zhang, *JOM* 70, 1430 (2018).
33. T.S. Kim, J.H. Park, and J. Non-Cryst, *Solids* 542, 120089 (2020).
34. J.S. Choi, T.J. Park, D.J. Min, and I. Sohn, *J. Mater. Res. Technol.* 15, 1382 (2021).
35. J.S. Choi, T.J. Park, and D.J. Min, *J. Am. Ceram. Soc.* 104, 140 (2021).